Alerts in High-resolution TEM characterization of perovskite material

Yu-Hao Deng[1*]

[1] Academy for Advanced Interdisciplinary Studies, Peking University, Beijing, China

* Correspondence should be addressed to yuhaodeng@pku.edu.cn

Abstract

High-resolution TEM (HRTEM) is a powerful tool for structure characterization. However, $MAPbI_3$ perovskite is highly sensitive to electron beams and easily decompose into PbI_2. Universal mistakes that PbI_2 is incorrectly labeled as perovskite are widely exist in HRTEM characterizations, which negatively affect the development of perovskite research field. Here complete errors in $MAPbI_3$ perovskite calibration are statisticed, classified and identified based on corresponding electron diffraction (ED) simulations. Corrected material phases, ED patterns of original PbI_2 and obvious crystallographic parameters are also presented. This approach paves the way to avoid misleadings in HRTEM characterization of perovskite and other electron beam-sensitive materials in the future.

Keywords: perovskite, $MAPbI_3$, transmission electron microscopy (TEM), electron diffraction (ED), phase calibration

Introduction

High-resolution transmission electron microscopy (HRTEM) is a very powerful characterization tool and has been extensively and successfully used for analyzing crystal structures on an atomic resolution scale [1]. Recently, halide perovskites have achieved substantial success in various optoelectronic devices owing to their solution-based growth method and remarkable physical properties[2-6]. However, $MAPbI_3$ perovskite is very sensitive

to electron beam irradiation. As a rough estimation, $MAPbI_3$ begins to decompose into PbI_2 under 150 $eÅ^{-2}$ total dose irradiation[7, 8]. Figure 1 shows the $MAPbI_3$ degradation process under electron beam irradiation. Tetragonal perovskite decomposes into hexagonal lead iodide by the escape of methylamine and hydrogen iodide molecules.

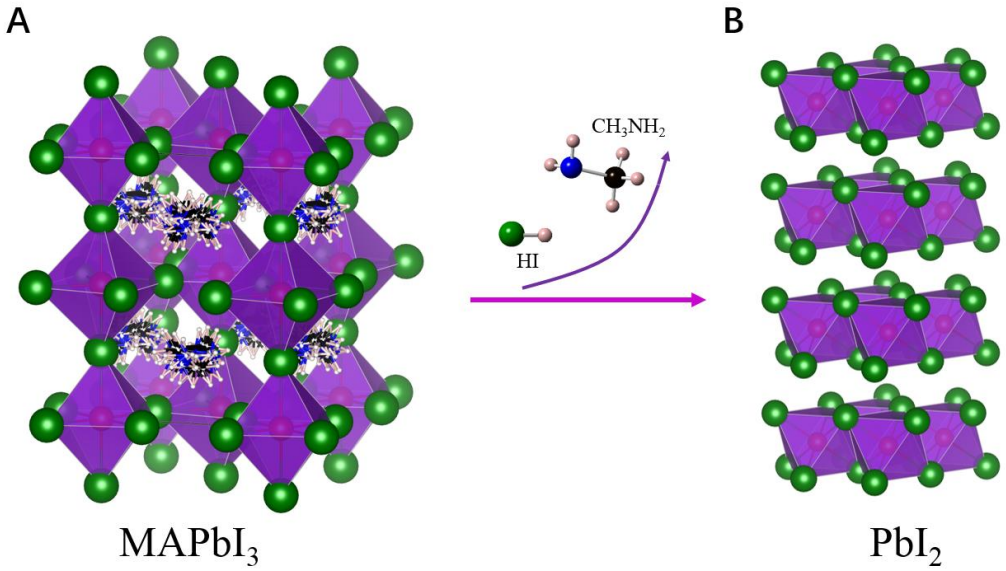

Fig. 1. $MAPbI_3$ degradation under electron beam irradiation. Tetragonal perovskite **(A)** decomposes into hexagonal lead iodide **(B)**, followed by the escape of methylamine and hydrogen iodide molecules. Here, colors represent the following: green, iodine; red, lead; black, carbon; blue, nitrogen; pink, hydrogen.

General phase calibration method of HRTEM data is to compare a group of interplanar spacings and angles. This method is easy to ignore the absent crystal planes and lead to mistaken calibration results, such as the lead iodide is generally labeled as perovskite. Although the mistakes are being taken seriously [7-9], a most complete summary and correction is still highly urgent.

Results and discussion

Here complete errors in $MAPbI_3$ perovskite calibration are statisticed, classified and corrected. Figure 2 shows simulated ED patterns of $MAPbI_3$ and PbI_2 along different axis zones. These crystal planes are often confused in perovskite calibrations. Figure 2A is the ED pattern of $MAPbI_3$ along [110] axis zone. $(\bar{1}10)$, (002) crystal planes are existing in a perfect tetragonal perovskite, but they are missing in HRTEM characterizations in previous research papers. The absence of crystal planes indicates that the material is no longer $MAPbI_3$ perovskite, but other

phases and structures. Figure 2B shows the simulated ED patterns of PbI_2 along [4$\bar{4}$1] axis zone. (014), ($\bar{1}$04) crystal planes of PbI_2 have the very closed interplanar spacing and angle with ($\bar{2}$20), (004) crystal planes of $MAPbI_3$. Actually $MAPbI_3$ has been damaged into PbI_2 phase by electron beams and neglect of the lack of crystal planes results in the mischaracterization. Similarly, Figure 2C-H are ED patterns of $MAPbI_3$ along [101] and PbI_2 along [8101], $MAPbI_3$ along [$\bar{2}$01] and PbI_2 along [8$\bar{8}$1], $MAPbI_3$ along [$\bar{1}$20] and PbI_2 along [$\bar{4}$11] respectively. Diffraction spots circled in red are missing crystal planes that were neglected in HRTEM characterizations. Moreover, these neglected planes are all present in X-ray diffraction (XRD) of $MAPbI_3$ [10-12].

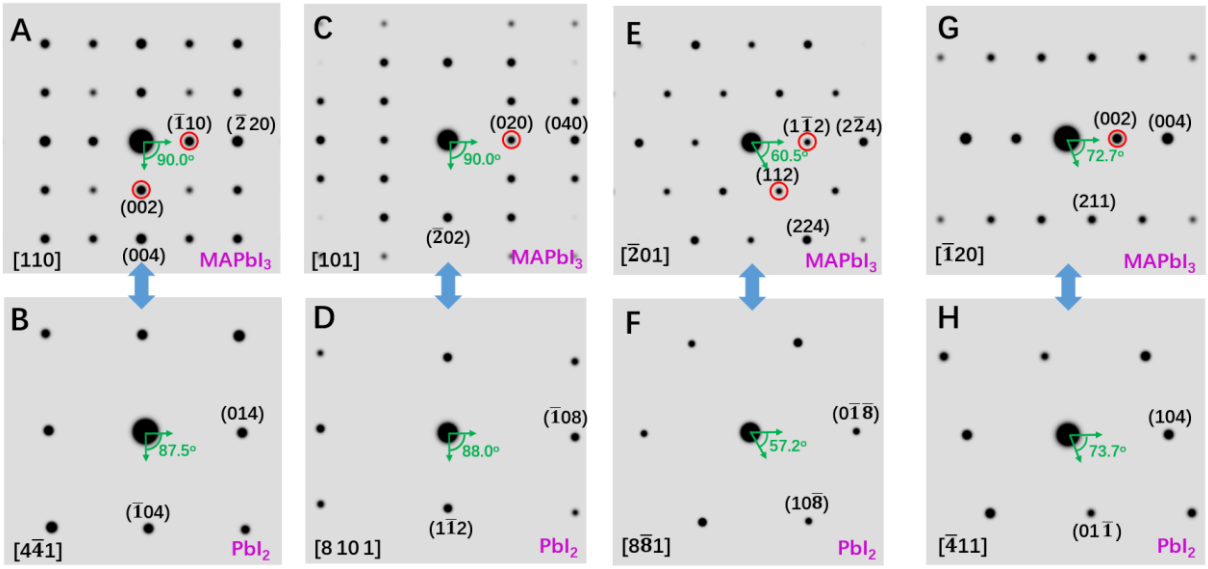

Fig. 2. Simulated electron diffraction (ED) patterns of tetragonal $MAPbI_3$ and hexagonal PbI_2. (A) $MAPbI_3$ along [110] axis zone. **(B)** PbI_2 along [4$\bar{4}$1] axis zone. **(C)** $MAPbI_3$ along [101] axis zone. **(D)** PbI_2 along [8 10 1] axis zone. **(E)** $MAPbI_3$ along [$\bar{2}$01] axis zone. **(F)** PbI_2 along [8$\bar{8}$1] axis zone. **(G)** $MAPbI_3$ along [$\bar{1}$20] axis zone. **(H)** PbI_2 along [$\bar{4}$11] axis zone. Crystal planes marked in red circle are often missing in published articles.

The mischaracterizations have negatively affected the development of perovskite scientific research field. Statistically, these errors occur in the following fields: phase identification and structure determination [13], grain, nanowire and microwire orientation [14-18], morphology analysis and shape control of nanocrystals [19], growth direction of perovskite materials [20], degradation process and kinetics of perovskite [21], phase transition research in perovskite [22] and ion migration characterization in photoelectric devices [23]. Not only in the field of single $MAPbI_3$ material system, misleading information also occurs in the research field of

heterostructure materials. Such as lattice matching and kinetic study in epitaxial growth of perovskite films on 2D material[24], PbS quantum dots in perovskite material[25, 26] and lattice anchoring stabilizes perovskite research[27]. To make the comparisons and corrections clearer, Table 1 shows the detailed parameters of the $MAPbI_3$ and PbI_2 along different axis zone, missing crystal planes have been marked in brown. Even remarkably, the [110] and [001] zone axis are equivalent in tetragonal $MAPbI_3$ perovskite.

Table 1. Detailed crystallographic parameters of $MAPbI_3$ and PbI_2.

Material and zone axis	Characteristic crystal planes	Interplanar spacing	Interplanar Angle	References
$MAPbI_3$ [110]	$(\bar{1}10)$, $(\bar{2}20)$ (002), (004)	d$(\bar{1}10)$= 6.2Å. d$(\bar{2}20)$= 3.1Å. d(002)= 6.3Å. d(004) =3.2Å.	<$(\bar{1}10)$, (002)> = <$(\bar{2}20)$, (004)> =90.0°	13-24
PbI_2 [4$\bar{4}$1]	(014) $(\bar{1}04)$	d(014)= 3.2Å. d$(\bar{1}04)$ =3.2Å.	<(014), $(\bar{1}04)$> =87.5°	_____
$MAPbI_3$ [101]	(020), (040) $(\bar{2}02)$	d(020)= 4.4Å. d(040)= 2.2Å. d$(\bar{2}02)$= 3.6Å.	<(020), $(\bar{2}02)$> = <(040), $(\bar{2}02)$> =90.0°	28, 29
PbI_2 [8 10 1]	$(\bar{1}08)$ $(1\bar{1}2)$	d$(\bar{1}08)$= 2.2Å. d$(1\bar{1}2)$= 3.7Å.	<$(\bar{1}08)$, $(1\bar{1}2)$> =88.0°	_____
$MAPbI_3$ [$\bar{2}$01]	$(1\bar{1}2)$, $(2\bar{2}4)$ (112), (224)	d$(1\bar{1}2)$= 4.4Å. d$(2\bar{2}4)$= 2.2Å. d(112)= 4.4Å. d(224)= 2.2Å.	<$(1\bar{1}2)$, (112)> = <$(2\bar{2}4)$, (224)> =60.5°	15, 25-27
PbI_2 [8$\bar{8}$1]	$(0\bar{1}\,\bar{8})$ $(10\bar{8})$	d$(0\bar{1}\,\bar{8})$= 2.2Å. d$(10\bar{8})$= 2.2Å.	<$(0\bar{1}\,\bar{8})$, $(10\bar{8})$ > =57.2°	_____
$MAPbI_3$ [$\bar{1}$20]	(002), (004) (211)	d(002)= 6.3Å. d(004) =3.2Å. d(211)= 3.8Å.	<(002), (211)> = <(004), (211)> =72.7°	30-33
PbI_2 [$\bar{4}$11]	(104) $(01\bar{1})$	d(104)= 3.2Å. d$(01\bar{1})$= 3.9Å.	<(104), $(01\bar{1})$> =73.7°	_____

Conclusions

Above statistics and corrections are very helpful for researchers to avoid mistakes in perovskite

research field. Others that incorrectly label metallic lead as perovskite can also be identified and corrected using the same method [34]. Lessons learned from the mistakes alert us it is unreliable to calibrate material phase only by measuring interplanar spacings and angles. We also need to refer simulated ED or XRD specimen data to ensure the crystal planes are complete. In addition, low dose irradiation [7, 35, 36] and low temperature [8, 37] can reduce the damage of electron beam irradiation to perovskite, and may help us get the real structure of perovskite materials. A solid method of phase identification can help us avoid the mistakes has also been proposed [38]. This work provides a sober-minded brain for further characterization in organic-inorganic hybrid perovskite and other electron beam-sensitive materials.

Methods

Corresponding crystal structures cif files were downloaded from Crystallography Open Database (COD) website. COD IDs of $MAPbI_3$ and PbI_2 are 4124388 and 9009141 respectively. $MAPbI_3$ is I4/mcm space group with tetragonal structure, cell parameters: a=b=8.839Å, c=12.695Å; $\alpha=\beta=\gamma=90^o$. PbI_2 is P-3m1 space group with hexagonal structure, cell parameters: a=b=4.555Å, c=20.937Å; $\alpha=\beta=90^o$, $\gamma=120^o$. The Electron diffraction (ED) simulations of $MAPbI_3$ and PbI_2 were obtained using CrystalMaker Software. The interplanar spacing and interplanar angle can be calculated from the cell parameters.

Data availability: All data are available from the corresponding author(s) upon reasonable request.

Conflict of interest: The authors declare no competing financial interest.

References

[1]. Jia C L, Lentzen M, Urban K. Atomic-resolution imaging of oxygen in perovskite ceramics[J]. Science, 2003, 299(5608): 870-873.

[2]. https://www.nrel.gov/pv/cell-efficiency.html, Best Research-Cell Efficiencies, National Renewable Energy Laboratory, accessed: 7, 2020.

[3]. Lin K, Xing J, Quan L N, et al. Perovskite light-emitting diodes with external quantum efficiency exceeding 20 per cent[J]. Nature, 2018, 562(7726): 245-248.

[4]. Yang Z, Deng Y, Zhang X, et al. High-Performance Single-Crystalline Perovskite Thin-Film Photodetector[J]. Advanced Materials, 2018, 30(8): 1704333.

[5]. Deng Y H, Yang Z Q, Ma R M. Growth of centimeter-scale perovskite single-crystalline thin film via surface engineering[J]. Nano convergence, 2020, 7(1): 1-7.

[6]. Zhu H, Fu Y, Meng F, et al. Lead halide perovskite nanowire lasers with low lasing thresholds and high quality factors[J]. Nature materials, 2015, 14(6): 636-642.

[7]. Chen S, Zhang X, Zhao J, et al. Atomic scale insights into structure instability and decomposition pathway of methylammonium lead iodide perovskite[J]. Nature communications, 2018, 9(1): 1-8.

[8]. Li Y, Zhou W, Li Y, et al. Unravelling degradation mechanisms and atomic structure of organic-inorganic halide perovskites by cryo-EM[J]. Joule, 2019, 3(11): 2854-2866.

[9]. Chen S, Gao P. Challenges, myths, and opportunities of electron microscopy on halide perovskites[J]. Journal of Applied Physics, 2020, 128(1): 010901.

[10]. Dong Q, Fang Y, Shao Y, et al. Electron-hole diffusion lengths> 175 μm in solution-grown $CH_3NH_3PbI_3$ single crystals[J]. Science, 2015, 347(6225): 967-970.

[11]. Mei A, Li X, Liu L, et al. A hole-conductor–free, fully printable mesoscopic perovskite solar cell with high stability[J]. Science, 2014, 345(6194): 295-298.

[12]. Shi D, Adinolfi V, Comin R, et al. Low trap-state density and long carrier diffusion in organolead trihalide perovskite single crystals[J]. Science, 2015, 347(6221): 519-522.

[13]. Yang M, Zhou Y, Zeng Y, et al. Square-centimeter solution-processed planar $CH_3NH_3PbI_3$ perovskite solar cells with efficiency exceeding 15%[J]. Advanced Materials, 2015, 27(41): 6363-6370.

[14]. Xiao M, Huang F, Huang W, et al. A fast deposition-crystallization procedure for highly efficient lead iodide perovskite thin-film solar cells[J]. Angewandte Chemie International Edition, 2014, 53(37): 9898-9903.

[15]. Yang B, Dyck O, Poplawsky J, et al. Controllable Growth of Perovskite Films by Room-Temperature Air Exposure for Efficient Planar Heterojunction Photovoltaic Cells[J]. Angewandte Chemie International Edition, 2015, 54(49): 14862-14865.

[16]. Son D Y, Lee J W, Choi Y J, et al. Self-formed grain boundary healing layer for highly efficient $CH_3NH_3PbI_3$ perovskite solar cells[J]. Nature Energy, 2016, 1(7): 1-8.

[17]. Zhu H, Fu Y, Meng F, et al. Lead halide perovskite nanowire lasers with low lasing thresholds and high quality factors[J]. Nature materials, 2015, 14(6): 636-642.

[18]. Li S, Li Y, Shi Z, et al. Fabrication of morphology-controlled and highly-crystallized perovskite microwires for long-term stable photodetectors[J]. Solar Energy Materials and Solar Cells, 2019, 191: 275-282.

[19]. Zhu F, Men L, Guo Y, et al. Shape evolution and single particle luminescence of organometal halide perovskite nanocrystals[J]. ACS nano, 2015, 9(3): 2948-2959.

[20]. Gao L, Zeng K, Guo J, et al. Passivated single-crystalline $CH_3NH_3PbI_3$ nanowire photodetector with high detectivity and polarization sensitivity[J]. Nano letters, 2016, 16(12): 7446-7454.

[21]. Fan Z, Xiao H, Wang Y, et al. Layer-by-layer degradation of methylammonium lead tri-iodide perovskite microplates[J]. Joule, 2017, 1(3): 548-562.

[22]. Li D, Wang G, Cheng H C, et al. Size-dependent phase transition in methylammonium lead iodide perovskite microplate crystals[J]. Nature communications, 2016, 7(1): 1-8.

[23]. Kim S, Bae S, Lee S W, et al. Relationship between ion migration and interfacial degradation of $CH_3NH_3PbI_3$ perovskite solar cells under thermal conditions[J]. Scientific reports, 2017, 7(1): 1-9.

[24]. Tang G, You P, Tai Q, et al. Solution-Phase Epitaxial Growth of Perovskite Films on 2D Material Flakes for High-Performance Solar Cells[J]. Advanced Materials, 2019, 31(24): 1807689.

[25]. Ning Z, Gong X, Comin R, et al. Quantum-dot-in-perovskite solids[J]. Nature, 2015, 523(7560): 324-328.

[26]. Gong X, Yang Z, Walters G, et al. Highly efficient quantum dot near-infrared light-emitting diodes[J]. Nature Photonics, 2016, 10(4): 253-257.

[27]. Liu M, Chen Y, Tan C S, et al. Lattice anchoring stabilizes solution-processed semiconductors[J]. Nature, 2019, 570(7759): 96-101.

[28]. Kim T W, Uchida S, Matsushita T, et al. Self-Organized Superlattice and Phase Coexistence inside Thin Film Organometal Halide Perovskite[J]. Advanced Materials, 2018, 30(8): 1705230.

[29]. Wang G, Li D, Cheng H C, et al. Wafer-scale growth of large arrays of perovskite microplate crystals for functional electronics and optoelectronics[J]. Science advances, 2015, 1(9): e1500613.

[30]. Niu L, Liu X, Cong C, et al. Controlled synthesis of organic/inorganic Van der waals solid for tunable light–matter interactions[J]. Advanced materials, 2015, 27(47): 7800-7808.

[31]. Liu X, Niu L, Wu C, et al. Periodic Organic–Inorganic Halide Perovskite Microplatelet Arrays on Silicon Substrates for Room-Temperature Lasing[J]. Advanced Science, 2016, 3(11): 1600137.

[32]. Kim T W, Shibayama N, Cojocaru L, et al. Real-time in situ observation of microstructural change in organometal halide perovskite induced by thermal degradation[J]. Advanced Functional Materials, 2018, 28(42): 1804039.

[33]. Zhao J, Kong G, Chen S, et al. Single crystalline CH3NH3PbI3 self-grown on FTO/TiO2 substrate for high efficiency perovskite solar cells[J]. Science Bulletin, 2017, 62(17).

[34]. Wang T, Zhang H, Hou S, et al. Facile synthesis of methylammonium lead iodide perovskite with controllable morphologies with enhanced luminescence performance[J]. Nanomaterials, 2019, 9(12): 1660.

[35]. Zhang D, Zhu Y, Liu L, et al. Atomic-resolution transmission electron microscopy of electron beam–sensitive crystalline materials[J]. Science, 2018, 359(6376): 675-679.

[36]. Chen S, Zhang Y, Zhao J, et al. Transmission electron microscopy of organic-inorganic hybrid perovskites: myths and truths[J]. Science Bulletin, 2020.

[37]. Zhu Y, Gui Z, Wang Q, et al. Direct atomic scale characterization of the surface structure and planar defects in the organic-inorganic hybrid $CH_3NH_3PbI_3$ by Cryo-TEM[J]. Nano Energy, 2020: 104820.

[38]. Deng Y H. Analysis of misidentifications in TEM characterization of perovskite material[J]. arXiv preprint arXiv:2009.04086, 2020. https://arxiv.org/abs/2009.04086